

On the Stability of Direct Spring-Operated Pressure Relief Valves: Impact of Frozen Mixture Flow and Lift Restriction

Ghaith Burhani^{1*}, Csaba Hős²

^{1,2} Budapest University of Technology and Economics, Department of Hydrodynamic Systems, Faculty of Mechanical Engineering, Műegyetem rkp 3., H-1111 Budapest, Hungary

Abstract: The current work explores the effect of (frozen) mixture flow and lift restriction on the stability of direct spring-operated pressure relief valves. First, we study the effect of frozen mixture (constant mass fraction) flow through a pressure relief valve with upstream piping. DIER's ω technique is employed to cope with the mixture parameters, notably sonic velocity and choked/non-choked flow through the nozzle. By means of one-dimensional simulation, we show that the change in sonic velocity plays a fundamental role in both the valve opening time and its stability. Due to the extremely low sonic velocities in certain range of water-air mass fraction, such valves will have a poor response time (slow opening) and chatter even for short inlet pipings. Next, we investigate the possibility of improving the dynamical performance of the safety valve by using a larger valve (i.e., a larger orifice) with a restricted lift option while keeping the vented mass flow rate through the valve constant. Our numerical investigations reveal that the additional restoring force emerging from the valve restriction at the upper stopper improves the stability behaviour in the case of gas applications but can hardly have any influence in the case of liquid service.

Keywords: safety valve, frozen mixture, sonic velocity, valve chatter, opening time, restricted lift.

Contents

1	Introduction	138
2	Literature review	139
3	Mathematical model	140
3.1	Frozen mixture model	140
3.2	Upstream pipe dynamics	141
3.3	Valve dynamics	142
3.4	Reservoir dynamics	143
3.5	Numerical solution procedure	143
4	Valve opening time	143
5	Instability thresholds	144
6	Restricted valves	145
6.1	Governing equations and data set	146
6.2	Stability of restricted valves	146
7	Conclusion	148

1 Introduction

Pressure relief valves (PRVs) are devices protecting the pipeline system and reservoirs from excess pressure by venting the unnecessary amount of fluid if needed. As such, they are safety-critical devices; inadequate operation (such as insufficient venting capacity, vibration, the inability of opening due to stuck parts) leads to catastrophic consequences.

These valves are essentially 1 DoF oscillators coupled with the fluid dynamics inside the piping system, resulting in a surprisingly rich dynamical behaviour; see, e.g., Hős et al. (2017) for an overview. It is well-known that such valves are prone to self-excited oscillations, see, e.g., (Kasai (1968); Bazsó and Hős (2013); Moussou et al. (2010); Singh (1983, 1982)), and a significant effort was devoted to predicting instabilities and oscillations in the phase of design (see, e.g., Darby (2012); Hős et al. (2014); Izuchi (2010); Melham (2014)). One of the cornerstones of such an analysis is the high-fidelity yet relatively simple description of

* E-mail address: gburhani@hds.bme.hu

the flow force on the valve body and the mass flow rate through the PRV. Although there are standard approaches to describe these forces – e.g. the "effective area" technique introduced in [H6s et al. \(2014\)](#) or the use of the jet angle as in [Darby \(2012\)](#); [Narabayashi et al. \(1986\)](#) – mostly single-phase cases (either pure gas or liquid) are addressed. [Boccardi et al. \(2005\)](#); [Dempster and Alshaikh \(2015\)](#); [Kourakos et al. \(2013\)](#); [Narabayashi et al. \(1986\)](#); [Dempster and Alshaikh \(2015\)](#) report on the effect of the two-phase flow on the *static* characteristics (flow force and mass flux) of the valve. However, the authors are unaware of any study trying to capture the effect of multiphase flow on the *dynamic* behaviour of a PRV (notably opening and closing characteristics) or to predict the effect of restricted valve lift.

This paper addresses the problem of predicting the dynamic behaviour of a PRV in the presence of two-phase flow of constant mass fraction and in the case of restricted-lift valves. As such, we do not consider phase change and the model will not be (directly) applicable for systems where interphase mass transfer is present (e.g. flashing flows). However, for multicomponent applications, in the absence of mass transfer between the components, our model will provide a possible description of the dynamics, for example in the case of bubbly flows, see, [Campagne et al. \(2002\)](#); [Ng and Yap \(1989\)](#); [Alimonti et al. \(2010\)](#), where, even though the void fraction changes if pressure changes, the mass fraction remains constant. Another example with constant mass fraction would be applications in which the humidity content of air is important, see, e.g., [Meena et al. \(2007\)](#) or [Kim et al. \(2016\)](#), especially Figure 8 therein.

The remainder of the paper is structured as follows. First, Section 2 provides a brief literature overview on safety valve dynamics, including valve chattering and DIER'S ω method. Next, we present our mathematical model of the frozen mixture in Section 3. Then, we show the simulation results on estimating valve opening time in Section 4 and valve stability in Section 5. Section 6 explores the impact of restricted valve lift on its stability. Finally, Section 7 summarizes and concludes the study.

2 Literature review

The problem of valve instability (i.e., chatter) has been known and studied since the 1980s, see, e.g. [Singh \(1982\)](#). Also, the relevant industrial standards, notably [API \(2015\)](#) codes, include guidelines for avoiding valve instabilities, leading to the so-called 3% rule, which claims to overcome the chatter problem by limiting the frictional (non-recoverable) pressure loss in the upstream piping.

[H6s et al. \(2014\)](#), address the analysis of the instabilities mechanisms of pressure relief valves in gas service, seeking to derive a model that considers the acoustic coupling between the valve and the pipe. This study revealed that the root cause of valve chatter is not the frictional pressure drop inside the upstream piping (even though it can also lead to vibrations) but the acoustic coupling between the first fundamental eigenmode ("organ" mode) of the pipeline. The proposed model and experimental results for three commercial valves, 1E2, 2J3, and 3LD, at different inlet mass flow rates and pipe lengths, showed a violent oscillation occurred beyond a critical pipe length even with negligible pipe friction.

[Makaryants \(2017\)](#) addressed a PRV self-excited oscillation mechanism in gas service. The authors tested the valve experimentally under external vibration conditions. Also, a verified mathematical model has been developed to reveal the nature of self-excited oscillations onset of PRV and predicts the valve dynamics. The empirical study indicated a low-frequency self-excited oscillation occurs in the range of 1 – 10Hz. However, other tested valves showed their failure tendency at high-frequency self-excited oscillations in the range of 100 – 120Hz. The failure is due to the acoustic coupling between the vessel and the pipe, which results in valve chatter. Finally, the proposed model prevents the undesired high-frequency self-excited oscillations and allows the appropriate value of friction force needed to eliminate chatter in all valve operating modes.

[Zheng et al. \(2021\)](#) report the dynamic instability of a spring-loaded PSV in gas service. A high-fidelity (CFD) model containing a PSV, different connected pipes, and the pressure vessel is proposed to investigate the influence of the rate of the vessel pressure rises, the stem friction, and the connecting pipe length. Furthermore, the acoustic waves along the connecting pipes are successfully captured, assessing the instability mechanism and optimizing the design and the setup of pressure relief systems. The authors found that increasing the vessel pressure rise rate opens the valve faster and reduces the valve disk oscillations, leading to increases in overpressure values. Moreover, increasing the stem friction improves the sensitivity of PSVs, but it increases the blowdown of the valve. Finally, the expansion/compression wave is reflected as a compression or expansion wave at the vessel. The latter runs back to the nozzle to enhance/weaken the flutter and chatter of the disk, which with a proper connecting pipe length, plays a positive role in the stability of the vessel-inlet pipe-safety valve system.

Pressure relief valves are sized and chosen based on their capacity, where the vented mass flow rate is at full opening and 110% of the set (opening) pressure. For ideal gas or incompressible liquid, it is straightforward to compute the mass flow rate if the valve lift (flow-through area) and the pressure difference (or, in the case of choked flow, the upstream pressure) are known, together with the discharge coefficient (provided by the manufacturer). However, predicting the mass flow rate is challenging in the case of wet steam, non-ideal gases or mixtures, or flashing (partial evaporation of saturated liquid due to pressure drop via the valve). DIER'S ω technique is one attempt to cope with this problem that assumes both thermal and mechanical homogeneous case and also neglects the velocity difference between the phases (no slip). Due to its popularity, we will employ this model, even though there are other, more accurate (and complex) models, such as TPHEM, HNE, and HDI methods (see, e.g., [Darby \(2005\)](#) for details).

In contrast to the single-phase flow, the two-phase case has one additional degree of freedom, that is the mass fraction of one of the phases; where gas mass fraction is $x_g = \dot{m}_g / (\dot{m}_g + \dot{m}_l)$ and the liquid mass fraction denoted by $x_l = \dot{m}_l / (\dot{m}_g + \dot{m}_l)$. \dot{m}_g and \dot{m}_l are the mass flow rates of the gas and liquid in the mixture, respectively.

Leung published a series of papers on the development and use of the ω technique. In [Leung \(1986\)](#), the author presented the generalised correlation for one-component homogeneous equilibrium model (HEM) for flashing choked flow validated against measurement results for eleven fluids with different properties. The key idea was that the flashing two-phase mixture was considered as a single-phase compressible fluid, and then the use of the ω parameter already defined by [Epstein et al. \(1983\)](#) for all-liquid mixtures. [Leung and Grolmes \(1988\)](#) extended the previous correlation for the flashing choked flow of an initially sub-cooled liquid (for both high and low sub-cooling regions), neglecting the effects of non-equilibrium effects and obtained design charts that were useful for practical applications. Leung discussed similarities between flashing and non-flashing two-phase flow in [Leung \(1990\)](#) and showed that, by simply redefining the dimensionless ω parameter, a unified treatment could be obtained.

In another study, [Leung and Nazario \(1990\)](#) reviewed three methods; (a) DIERS' ω method, (b) a technique used by the American Petroleum Institute (API) and (c) the American Society of Mechanical Engineering (ASME) code, to compare the mass flux of flashing flow. These methods are widely used in various engineering applications. It has been found the ASME and DIERS' ω models are in close agreement. Also, the API method gives significantly higher theoretical mass flux values since it neglects momentum, heat and mass transfer during the flashing process.

Leung also summarised his previous works in [Leung \(1995\)](#), covering the ω method for mass flux estimation both for ideal nozzle flow and pipe flow with different orientations (horizontal and inclined pipe flows), for flashing, non-flashing, inlet sub-cooled and non-condensable gas. Nine years later, he applied the ω method for safety relief valves, see, [Leung \(2004\)](#). It was also shown how the discharge coefficient varies depending on the flow regime, and it was revealed that for the non-flashing flow case, the discharge coefficient lies between the liquid coefficient and the gas coefficient. Moreover, the author observed a higher discharge coefficient value in the flashing flow case than in the single-gas case. [Lees \(2012\)](#) proposed techniques for employing the ω model based on the stagnation conditions of fluid in the vessel and discussed four main cases; saturated liquid, two-phase (gas-liquid mixture), low sub-cooled liquid, and high sub-cooled liquid.

[Lenzing et al. \(1998\)](#) studied experimentally the effect of two-phase flow (flashing and non-flashing) on the capacity at the maximum lift of the valve. The authors compared the measured data against several theoretical predictions, namely the DIERS' ω technique, Nastoll's Homogeneous Frozen Flow model and the Goßlau-Weyl model. The results showed that for non-flashing flow ω method is the most powerful technique and was superior to the rest of the employed models (see Figure 1. in [Lenzing et al. \(1998\)](#) and the corresponding text).

Last but not least, [Boccardi et al. \(2005\)](#) discussed measured data of (steam/water) flashing flow through a PRV with a wide range of operating parameters such as vapour quality, inlet pressure, mass flow rate, and backpressure. The measurement data was examined against HEM ω method, and the results showed that the mass flow rates provided by ω model and the actual (measured) flow rates correlated reasonably. Later, the same authors in another work, [Boccardi et al. \(2010\)](#) compared the experimental data of steam-water flow against three models: HEM (homogeneous equilibrium model), HNE (thermodynamic non-equilibrium) and HNE-DS (proposed by the ISO working group). The results revealed that, even though the HNE-DS method provided the best results, it was not conservative in some cases as it gave higher flow rates than the measurements. In contrast, the HEM (DIERS' ω) technique showed poor accuracy but was conservative.

Based on the theoretical and experimental work published in the above reports, Leung's ω technique provides a reasonable compromise between modelling complexity and prediction accuracy and we will employ this approach in this paper.

3 Mathematical model

3.1 Frozen mixture model

Consider the frozen mixture of an ideal gas and a liquid, that is the gas mass fraction $x_g = \frac{\dot{m}_g}{\dot{m}_m} = \frac{\dot{m}_g}{\dot{m}_m}$ is constant, where $\dot{m}_m = \dot{m}_g + \dot{m}_l$ is the mixture flow rate and, clearly, $x_l = 1 - x_g$.

We assume that the gas obeys the ideal gas law, that is, $p/\rho_g = RT$, where p stands for the pressure, T is the absolute temperature (K), R is the specific gas constant, and ρ_g denotes the gas density. For an isentropic change of state, the sonic velocity for pure gas ($x_g = 1$) is $a_g = \sqrt{\kappa RT}$ and κ is the adiabatic exponent of the gas (e.g. $\kappa = 1.4$ for air). The equation of state of the liquid phase describes the liquid density is

$$\rho_l = \rho_{ref} + \frac{1}{a_l^2} (p - p_{ref}), \quad (1)$$

where the reference values are the reference pressure $p_{ref} = 1 \text{ bar}$, the liquid (water) reference density $\rho_{ref} = 1000 \text{ kg/m}^3$, and a_l is the sonic velocity measured in pure liquid.

The α_g volume fraction is

$$\alpha_g = \frac{V_g}{V_g + V_l} = \frac{m_g}{m_g + m_l \frac{\rho_g}{\rho_l}} = \frac{x_g}{x_g + (1 - x_g) \frac{\rho_g}{\rho_l}}, \quad (2)$$

where V_g , V_l , m_g , and m_l are gas volume, liquid volume, gas mass, and liquid mass in the frozen mixture, respectively.

The mixture density $\rho_m(p, T, x_g)$ becomes

$$\begin{aligned} \rho_m &= \frac{m_m}{V_m} = \frac{\rho_g V_g + \rho_l V_l}{V_g + V_l} = \alpha_g \rho_g + (1 - \alpha_g) \rho_l \\ &= \frac{p(p - p_{ref} + a_l^2 \rho_{ref})}{(p_{ref} - p)RTx_g + a_l^2(p(x_g - 1) - RTx_g \rho_{ref})}, \end{aligned} \quad (3)$$

where V_m stands for the mixture volume.

It is easy to check that $\rho_m(x_g = 1) = \frac{p}{RT}$ and setting $x_g = 0$ recovers Eq. (1). We will also need the pressure as a function of temperature, (mixture) density and gas mass fraction $p(\rho_m, T, x_g)$, which is

$$\begin{aligned} p &= \frac{1}{4} \left(-b + \sqrt{b^2 - 4c} \right), \quad \text{with} \\ b &= - \left(p_{ref} + RTx_g \rho_m + a_l^2 (\rho_m(1 - x_g) - \rho_{ref}) \right), \quad \text{and} \\ c &= RTx_g \rho_m \left(p_{ref} - a_l^2 \rho_{ref} \right). \end{aligned} \quad (4)$$

Now we are in the position of computing the mixture sonic velocity. First, we eliminate the temperature dependence from Eq. (3) by assuming isentropic change of state for the gas, and then compute

$$\begin{aligned} a_m^2 &= \left(\frac{d\rho_m(p, x_g)}{dp} \right)^{-1} \Big|_{isentropic} \\ &= \frac{\kappa (a_0 + a_1)^2}{b_0 + b_1 + b_2 + b_3}, \quad \text{where} \\ p &= p_{ref,g} \left(\frac{T}{T_{ref,g}} \right)^{\frac{\kappa}{\kappa-1}} \\ a_0 &= (p - p_{ref})RTx_g \\ a_1 &= a_l^2 (p(1 - x_g) + RTx_g \rho_{ref}) \\ b_0 &= -p^2 RTx_g \\ b_1 &= a_l^2 p^2 (x_g - 1) \\ b_2 &= 2pRTx_g (p_{ref} - a_l^2 \rho_{ref}) \\ b_3 &= -RTx_g (p_{ref} - a_l^2 \rho_{ref})^2. \end{aligned} \quad (5)$$

It is straightforward again to check that $a_m^2(x_g = 0) = a_l^2$ and $a_m^2(x_g = 1) = \kappa RT$. Fig. 1 depicts the change of sonic velocity (solid line) and gas void fraction α_g (dashed line) as a function of gas mass fraction. These results are in good agreement with the literature data, see, e.g., [Nguyen et al. \(1981\)](#) for example. The sonic velocity will play a central role in our further analysis, hence we highlight two well-known facts, namely that: (1) the sonic velocity can be as low as 20-50 m/s and (2) a relatively small amount of air (say, $x_g = 10^{-6}$, $\alpha_g = 8.3 \times 10^{-4}$) changes the sonic velocity drastically.

3.2 Upstream pipe dynamics

The governing equations for 1D unsteady flow of an arbitrary fluid in a tube of constant cross-section (that is, a pipe with D_p diameter and friction factor λ) are as follows

$$\frac{\partial \mathcal{U}}{\partial t} + \frac{\partial \mathcal{F}}{\partial x} = \mathcal{S}, \quad (6)$$

with

$$\mathcal{U} = \begin{pmatrix} \rho_m \\ \rho_m v \\ \rho_m v e_{tot} \end{pmatrix}, \quad \mathcal{F} = \begin{pmatrix} \rho_m v \\ \rho_m v^2 + p \\ \rho_m v e_{tot} + pv \end{pmatrix}, \quad \text{and} \quad \mathcal{S} = \begin{pmatrix} 0 \\ -\frac{\lambda}{2D_p} v|v| \\ 0 \end{pmatrix}, \quad (7)$$

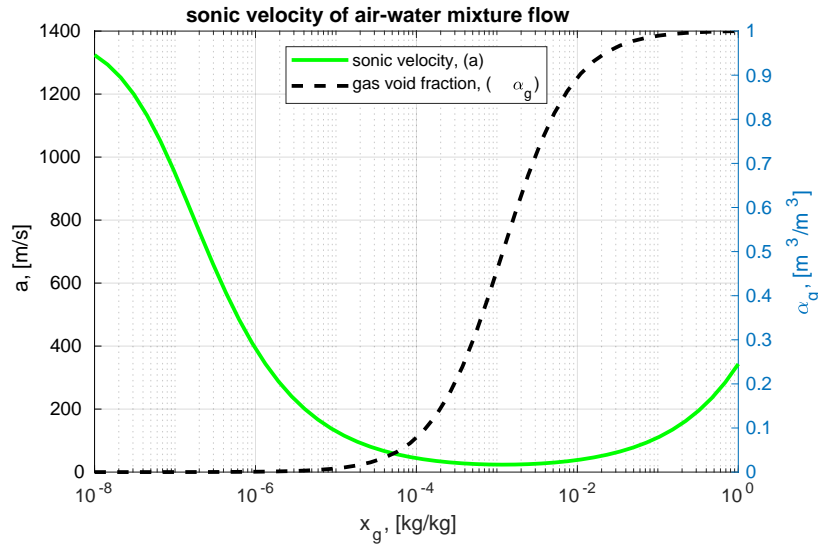


Fig. 1: Sonic velocity (left axis) and gas void fraction (right axis) as a function of gas mass fraction.

where the total energy e_{tot} is the sum of the internal energy e and kinetic energy $\frac{v^2}{2}$; hence, $e_{tot} = e + \frac{v^2}{2}$. The mixture internal energy is $e_m = e_g + e_l = c_{V,g}Tx_g + c_{V,l}T(1-x_g) = c_{V,m}T$, and each of e_g and e_l are the gas and liquid internal energy, respectively. Note that the mixture specific heat capacity at constant volume is $c_{V,m} = x_g c_{V,g} + c_{V,l}(1-x_g)$, where $c_{V,g}$ and $c_{V,l}$ denote the specific heat capacity of gas and liquid in the mixture content.

3.3 Valve dynamics

The valve is modelled by a simple 1 DoF oscillatory system, whose governing equation is given by

$$m_v \ddot{x} + k \dot{x} + s(x + x_0) = A_{eff}(\tilde{x}) A_v (p_u - p_b), \quad (8)$$

with m_v being the valve mass, s standing for the spring stiffness, and k is the viscous damping coefficient. A_v refers to the valve seat area, x_0 is the spring pre-compression, and x , \dot{x} , \ddot{x} denote the valve lift, velocity and acceleration, respectively. $A_{eff}(\tilde{x})$ is the dimensionless *effective area* curve as a function of the relative valve lift $\tilde{x} = \frac{4x}{D_p}$, which models the force component due to the momentum of the fluid (see Burhani and H6s (2020, 2021) for more details). The pressure difference $(p_u - p_b)$ contains the upstream pressure p_u and the backpressure p_b , which does not necessarily equal the ambient pressure p_a . By adjusting the x_0 spring pre-compression, one can change the opening or *set pressure* p_{set} , which, by definition, is a gauge pressure: $p_{set} = \frac{s x_0}{A_v} - p_a$. Pressure relief valves in oil and gas industry typically contain no artificial damping mechanism but only natural damping, hence we will set $k = 0.01 \times 2\sqrt{s m_v}$.

The mass flow rate through the valve is $\dot{m}_v = C_d A_{ft}(x) \sqrt{p_u \rho_u} \mathcal{G}(\eta)$, where C_d stands for the discharge coefficient, A_{ft} is the flow through area, ρ_u refers to the upstream fluid density, and $\mathcal{G}(\eta)$ is the *dimensionless* mass flux as a function of the pressure ratio $\eta = p_d/p_u$, and p_d is the downstream pressure. The *dimensionless* mass flux $\mathcal{G}(\eta)$ can be given as

for an incompressible fluid:

$$\mathcal{G}(\eta) = \sqrt{2(1-\eta)}. \quad (9)$$

for non-choked, single-phase ideal gas:

$$\mathcal{G}(\eta) = \sqrt{2 \frac{\kappa}{\kappa-1} (\eta^{2/\kappa} - \eta^{(\kappa+1)/\kappa})}. \quad (10)$$

for choked, single-phase ideal gas:

$$\mathcal{G}(\eta) = \sqrt{\kappa \left(\frac{2}{\kappa+1} \right)^{\frac{\kappa+1}{\kappa-1}}}. \quad (11)$$

for non-choked frozen mixture flow:

$$\mathcal{G}(\eta) = \frac{(-2(\omega \ln \eta + (\omega-1)(1-\eta)))^{1/2}}{\omega \left(\frac{1}{\eta} - 1 \right) + 1}. \quad (12)$$

for choked frozen mixture flow:

$$\mathcal{G}(\eta) = \frac{\eta_c}{\sqrt{\omega}}, \quad (13)$$

where the critical pressure ratio $\eta_c = \frac{p_c}{p_u}$ can be calculated by solving the following implicit equation:

$$\eta_c^2 + (\omega^2 - 2\omega)(1 - \eta_c)^2 + 2\omega^2 \ln \eta_c + 2\omega^2(1 - \eta_c) = 0. \quad (14)$$

and the compressible flow number $\omega = \alpha_g/\kappa$ in the case of frozen mixture flow, see [Leung \(1995\)](#).

3.4 Reservoir dynamics

The rate of change of pressure inside a reservoir of volume V_r is

$$\dot{p}_t = \frac{a_r^2}{V_r} (\dot{m}_{in} - \dot{m}_{out}). \quad (15)$$

We shall assume constant inlet flow rate \dot{m}_{in} and variable outlet flow rate \dot{m}_{out} , typically, through a pipeline. The reservoir sonic velocity a_r depends on the reservoir temperature, which is connected to the reservoir pressure p_r by an arbitrary, user-defined change of state (e.g. isentropic, isotherm, etc.).

3.5 Numerical solution procedure

We use a standard Lax-Wendroff scheme for updating the pipe. The boundary conditions are implemented with the help of Method of Characteristics (MoC, see [Anderson \(1995\)](#)), the details can be found in [Erdődi and Hős \(2017\)](#). The valve and reservoir model are integrated by a standard 5th-order adaptive Runge-Kutta solver. Special care is devoted to the proper handling of the valve impingement on the seat or upper stopper. The time step is chosen by the CFL criteria, with a CFL number of 0.7-0.9. The whole framework is implemented in Matlab 2021b.

4 Valve opening time

In [Burhani and Hős \(2020\)](#), an approximate formula was derived for 'fast' valve opening time. Let the timescale of the valve be $t_{valve} = 2\pi/\omega_v = 2\pi\sqrt{m/s}$, where ω_v stands for the eigenfrequency of valve. We define the opening time t_{op} as the time needed for a closed valve to reach the 95% of the equilibrium lift x_e for a prescribed mass flow rate \dot{m}_{in} . If $t_{op} \ll t_{valve}$, we have

$$t_{op} \approx 2 \times 0.95x_e\omega_v^2 \frac{m_v \sum V}{A_p a^2 \dot{m}_{in}}. \quad (16)$$

(The condition $t_{op} \ll t_{valve}$ or, equivalently, $\omega_v t_{op} \ll 2\pi$ must be checked a posteriori). The above equation was derived by assuming a valve mounted directly to the reservoir. Intuitively, a pipe between the valve and reservoir would add additional volume and, if long enough, it will give rise to wave phenomena that also increase the valve opening time. Hence we have $\sum V = V_r + A_p L_p$, where A_p is the pipe cross-section area and L_p denotes the pipe length.

We have run several computations to analyse the effect of the mass fraction on the valve opening time with the parameter values provided in Tab. 1. For the water case, we have set $V_r = 2\text{m}^3$ and the valve lift and pressure in equilibrium position were $x_e = 0.33\text{mm}$ and $p_e = 4.11\text{ bara}$, respectively. This gives (by virtue of Eq. (16)) $t_{op} = 0.0278\text{ s}$ for opening time. Fig. 2 depicts the first 0.05 s of the opening process with three different pipe lengths. The dashed horizontal line represents the equilibrium valve lift, and the asterisk is the estimated opening time. We observe a slightly increasing opening time due to the increasing pipe length, which changes the overall volume (capacity) in the system. The change in the opening time (Eq. (16)) due to the increasing pipe length is less than 1%. We also experienced "opening instability" (see [Hős et al. \(2014\)](#) for details). From the mechanical point of view, this case is under-damped as the maximum of the valve lift is 50% higher than the equilibrium position.

Tab. 1: Parameters

valve mass	m_v	0.2 kg
spring stiffness	s	47.3 kN/m
valve eigenfreq.	f_v	77 Hz
valve timescale	t_v	0.013 s
set pressure	p_{set}	3 bar(g)
pipe diameter	D_p	45.5 mm
pipe friction coeff.	λ	0.02
inlet mass flow rate	\dot{m}_{in}	0.77 kg/s

In the case of pure air, we have $V_r = 0.02\text{m}^3$, $x_e = 5.97\text{mm}$ and $p_e = 5.9\text{bara}$. This case is over-damped, even though the viscous damping parameter was unchanged and the reservoir volume is smaller; see Fig. 3. Again, the dashed line represents the equilibrium lift, and the asterisk depicts the opening time estimated by Eq. (16). In this case, we do not experience opening instability.

In both cases, the simulations with longer pipe lengths resulted in unstable valve motion, leads us to our next section.

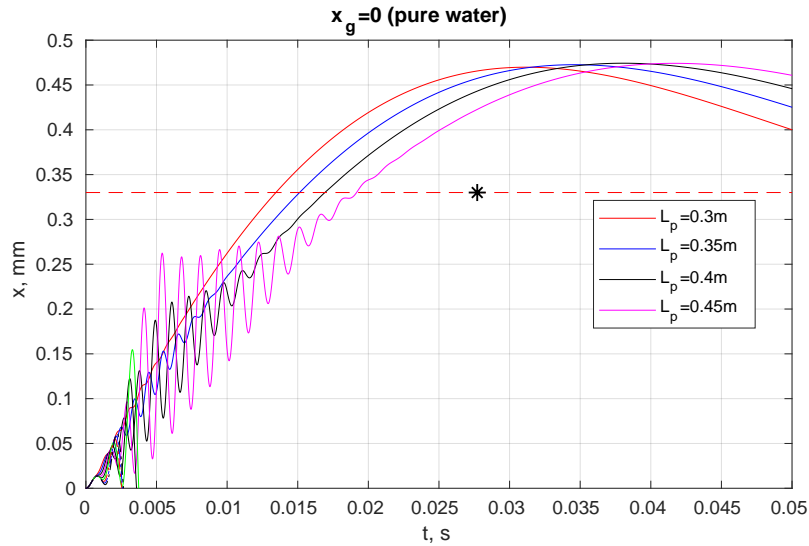


Fig. 2: Valve openings with different pipe lengths for pure water. The dashed line represents the equilibrium lift, and the asterisk depicts the opening time estimated by Eq. (16).

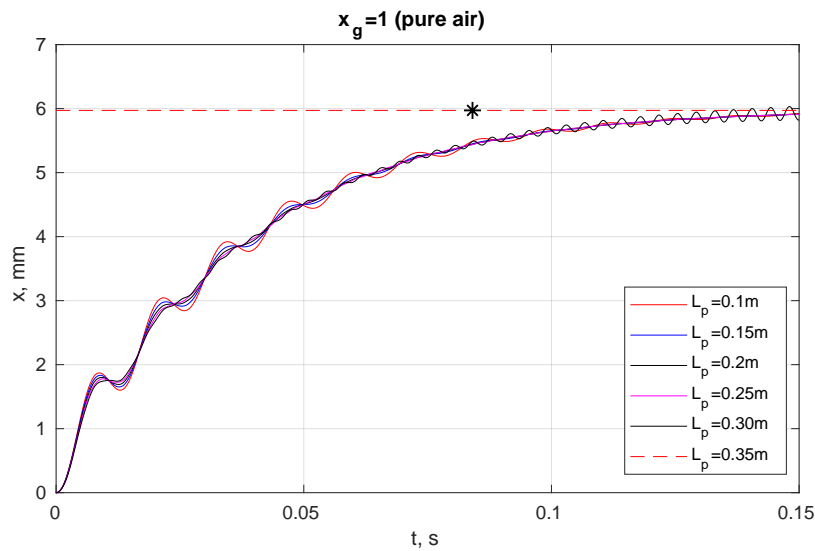


Fig. 3: Valve openings with different pipe lengths for pure air. The dashed line represents the equilibrium lift, and the asterisk depicts the opening time estimated by Eq. (16).

5 Instability thresholds

In Hős et al. (2016), the authors derived an analytical criteria for computing the critical inlet pipe length, that is

$$L_{crit} = \frac{\pi a}{2\omega_v} \frac{1}{\sqrt{2 \frac{A_v p_e}{x_e s} + 1}}, \tag{17}$$

where x_e and p_e are the equilibrium valve lift and (absolute) pressure at the valve inlet. Beyond the critical pipelength defined by the above equation, self-excited oscillations will be born, whose dominant frequency will coincide with the pipe’s first natural ‘organ-mode’ eigenfrequency, $f_p = a/(4L_p)$.

Izuchi (2010) provided a similar equation, that is

$$L_{crit}^* = \frac{\pi a}{2\omega_v} \frac{1}{\sqrt{\frac{x_e + x_0}{x_e}}}. \tag{18}$$

We notice that due to the force equilibrium of the valve, we have $s(x_e + x_0) = A_v(p_u - p_b)$, hence, if p_u is measured as a relative (gauge) pressure above p_b (which is often the ambient pressure), and the momentum forces can be neglected ($A_{eff} = 1$ in Eq. (8)), we have $\frac{A_v p_e}{x_e s} = \frac{x_e + x_0}{x_e}$, which is similar to Izuchi’s equation, but still, the factor of 2 and the +1 terms are missing.

We have run simulations with two set pressure, that is $p_{set} = 3$ barg and 15 barg. Fig. 4 and Fig. 5 depict the result. As it can be seen by virtue of Eq. (17), the critical pipe length depends on the equilibrium lift and pressure (x_e and p_e) and the sonic velocity.

The uppermost panels show the equilibrium lift: it remains constant up to $x_g \approx 0.01$, beyond which it increases due to the fact that the density of the mixture decreases but the overall vented mass flow rate is kept constant. We observe a similar trend in the case of the equilibrium pressure.

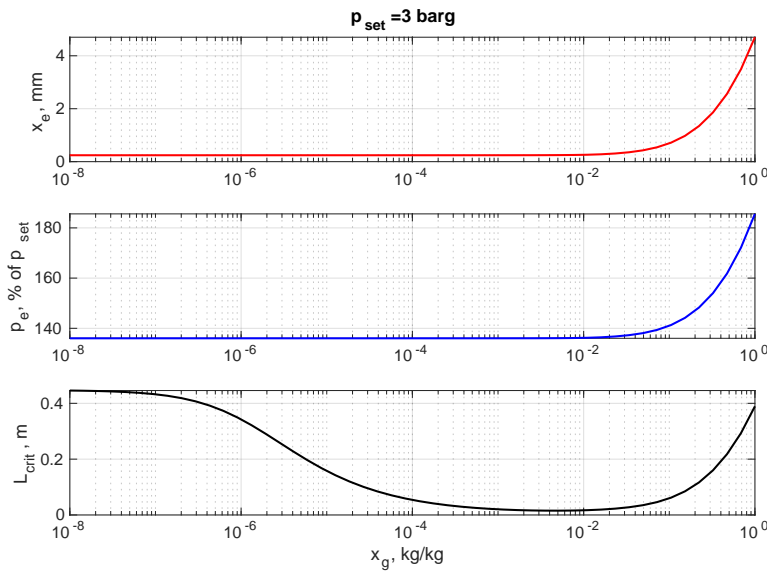


Fig. 4: Equilibrium lift, pressure and critical pipe length for $p_{set} = 3$ barg and $\dot{m}_{in} = 0.77$ kg/s.

However, the shape of the critical pipe length (bottom panels) resembles on the shape of the sonic velocity, see Fig. 1. More importantly, in the range of $x_g < 10^{-2}$, the equilibrium lift and pressure are constant yet the critical pipe length changes. This is another observation supporting the importance of the sonic velocity. Again, in the range of the low sonic velocity, the valve will be unstable basically for any (small) pipe length.

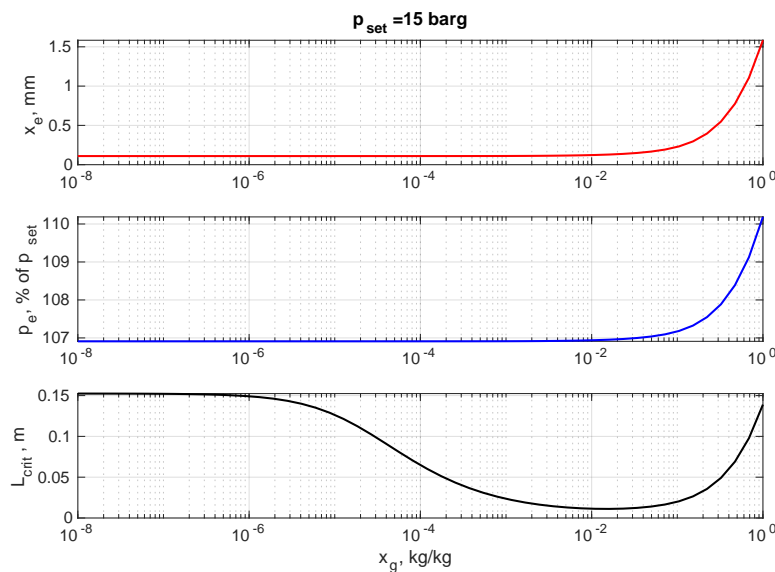


Fig. 5: Equilibrium lift, pressure and critical pipe length for $p_{set} = 15$ barg and $\dot{m}_{in} = 0.77$ kg/s.

6 Restricted valves

A well-known solution against excessive ($> 3\%$) inlet pressure drop and/or valve chatter is to employ a larger lift with restricted lift. For instance, some manufacturers, such as Baker Hughes, offer the Consolidated 1900 Series API 526 pressure relief valve with a restricted lift option (Hughes (2017)), which allows the adjustment of capacity in a secure and cost-effective way as only the washer needs to be added. Also, the lift restriction is more suitable to match the required capacity of the protected vessel or pipe with the actual and rated capacities of the relief valve, providing over-pressure protection. The inlet piping pressure losses and the acoustic wave effects will also be decreased, improving the stability of the safety valve performance (see, e.g., API (2015)). However, ASME Code and API 526 require that restriction not to be less than 30% of the PRV maximum (full) lift x_{max} or less than 2 mm.

Tab. 2: Crosby valve data. The restriction – see text below – is computed such that the restricted valve vents the capacity of the J orifice valve @ 110% of p_{set} .

orifice	J	K	L	M
orifice area $A_v = D_o^2\pi/4 \text{ mm}^2$	830	1186	1841	2323
$D_o, \text{ mm}$	32.5	38.9	48.4	54.4
$x_{max} = D_o/4, \text{ mm}$	8.12	9.71	12.1	13.6
capacity, air kg/s @ $p_{set} = 4 \text{ barg}$	0.97	1.38	2.14	2.70
required restriction ratio RT, %	0	30	54.9	64.3

Lift restriction is executed by installing a limit washer between the valve guide and disc holder, whose length should meet the required valve lift. Later, if the capacity is insufficient, only the location of the limit washer needs to be changed to get a larger capacity (larger orifice valve), see, e.g., (Hellemans (2009)).

Even though lift restriction is well-known in the industry, little work has been done on exploring its effect on the stability of the valve. In what follows, we present the results of a systematic parametric computation series on the effect of lift restriction. We shall search for the critical pipe length (instability threshold), beyond which the valve chatters for several valve (nozzle) sizes restricted such that the capacity (mass flow rate at 110% of set pressure and full - restricted - lift) is kept constant.

6.1 Governing equations and data set

We begin by establishing steady-state performance charts for restricted valves, which will be useful when analysing the stability properties. The valve flow rate is

$$\dot{m}_v = C_d A_{ft}(x) \sqrt{p_u \rho_u \mathcal{G}(\eta)}, \quad (19)$$

which was already explained in Section 3.3 ($\eta = p_d/p_u < 1$ is the pressure ratio). The flow-through area is $A_{ft}(x) = D_o \pi x$, where D_o is the orifice (often referred to as bore or nozzle) diameter and we shall emphasize that valves of different size will have different orifices: the data set for the Crosby standard valves is given in Tab. 2.

Restriction is the "infeasible" section of the valve lift given in percent of full lift (0% is unrestricted), and, by definition, capacity is the mass flow rate through the valve at $p_v = 110\%$ of p_{set} and maximum (possibly restricted) lift. Let us assume that we want to vent the capacity flow rate of valve with orifice A with a valve with orifice B , then, the required restriction is $RT(\%) = \left(1 - \frac{A_{o,A}}{A_{o,B}}\right) \times 100$, and the restricted maximum lift is $x_{max,RT} = (1 - RT/100)x_{max}$.

If the valve is restricted, an additional force component emerges at the upper stopper, which we shall refer to as restoring force F_r . Now, if the valve body is in contact with the upper stopper, the force balance reads

$$s(x_0 + x) = A_v (p_v - p_b) + F_r. \quad (20)$$

In what follows, we present the performance curves of restricted valves. However, due to some data being unavailable in the catalogues, some parameters were simply computed and might differ from the Crosby's actual data. We require that the valve opens at p_{set} , hence $sx_0 = A_v (p_a + p_{set} - p_b)$ (p_{set} is gauge pressure and the backpressure p_b might differ from the ambient pressure p_a). Also, the valve should reach full lift at $1.1p_{set}$, that is $s(x_0 + x_{max}) = A_v (p_a + 1.1 \times p_{set} - p_b)$. These two equations allow us to compute the required spring stiffness s and pre-compression x_0 for all valves in Tab. 2, giving different values for all orifice sizes and set pressures. Finally, the discharge coefficient C_d was set such that the capacity meets that data provided by Crosby.

After setting up the parameters we have plotted the mass flow rate of different valves as a function of the valve pressure p_v , in the range of $100\% \leq p_v/p_{set} \leq 115\%$, as show in Fig. 6. The upper figure depict the mass flow rate (relative to the capacity of the J orifice) vs. the pressure (gauge, relative to the set pressure). Notice that the spring stiffness and spring precompressions are set such that all valves have 100% of capacity at 110% of set pressure. Valve J reaches full lift and capacity at 110% of set pressure, while the rest of the valves reach full lift earlier (at the sudden slope change of the curves) and beyond that point, the valve lift is fixed yet the flow rate slightly increase as the pressure difference increase. Once the valve is fully open, the restoring force (bottom figure) increases as the pressure increases. For example, at 106% of p_{set} , valve with orifice J reaches approx. 60% of its capacity (the valve is not fully open), valve with orifice K reaches approx. 90% of the capacity, while orifices K and L almost reach full capacity plus experience approx. 10 and 20 N of restoring force. Our working hypothesis at this point is that the restoring force helps in stabilizing the valves against chatter.

6.2 Stability of restricted valves

We have tested the performance of the valves (numerically). Initially, the valve was closed and the incoming flow rate into the reservoir ($\dot{m}_{r,in}$) was kept constant over the entire simulation. The actual flow rate was chosen to match the capacity of the valve with J orifice at the prescribed set pressure. We have run several tests but only two representative cases are depicted here. The first

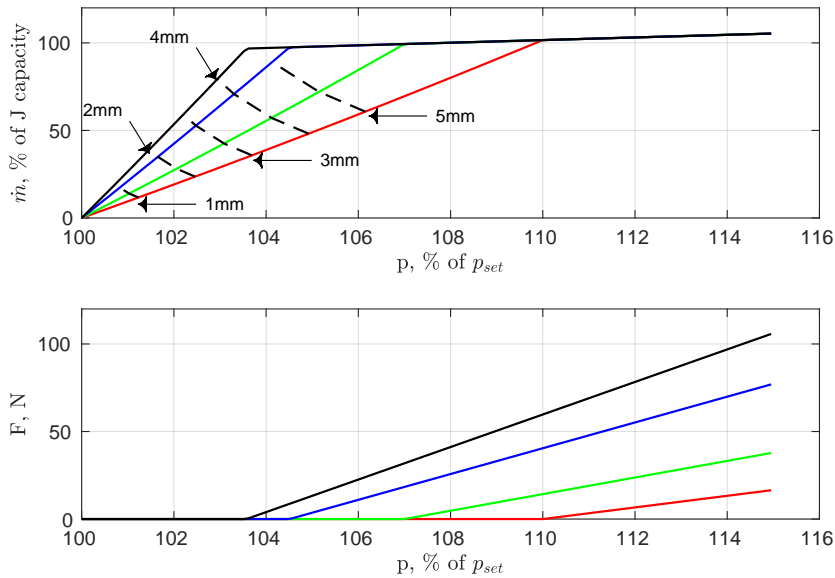


Fig. 6: Mass flow rate (relative to the capacity of the J orifice valve at $p_{set} = 4\text{barg}$) vs. valve pressure for valves with orifice J (red), K (green), L (blue) and M (black). The dashed lines are the data points at absolute lifts (e.g., 1, 2, 3, 4, and 5 mm). Note that for valve with orifice M, the maximum lift is $x_{max} = 4.89\text{ mm}$ at $RT = 64.3\%$, so there is no data reported in the figure at the absolute lift 5 mm.

set of computations were performed under air service at 4, 10, and 50 barg of p_{set} , while the second series of computations were assuming water service with the same set pressures.

In order to test the improvement in stability, we also compute the critical pipe length according to Eq. (17). For the air service case, we have $m_v = 0.2\text{kg}$, $s = 4.08\text{kN/m}$, giving $\omega_v = 143\text{rad/s}$ (22.7 Hz). The sonic velocity in air at room temperature is $a = 343\text{m/s}$ and the reservoir volume is assumed to be $V_r = 0.5\text{m}^3$. At full lift, $p_e = p_a + 1.1 \times p_{set} = 5.4\text{bar}$ and $x_e = x_{max} = 8.12\text{mm}$, which gives

$$L_{crit,air} = \frac{\pi a}{2\omega_v} \frac{1}{\sqrt{2 \frac{A_v p_e}{x_e s} + 1}} = 0.71\text{m} \quad (\text{orifice: J, } p_{set} = 4\text{barg}). \tag{21}$$

In the case of water service – $a = 1300\text{m/s}$, $p_{set} = 50\text{barg}$, $s = 51\text{kN/m}$, $\omega_v = 505\text{rad/s}$ (80.4 Hz), $V_r = 5\text{m}^3$ – we obtain

$$L_{crit,water} = \frac{\pi a}{2\omega_v} \frac{1}{\sqrt{2 \frac{A_v p_e}{x_e s} + 1}} = 0.83\text{m} \quad (\text{orifice: J, } p_{set} = 50\text{barg}). \tag{22}$$

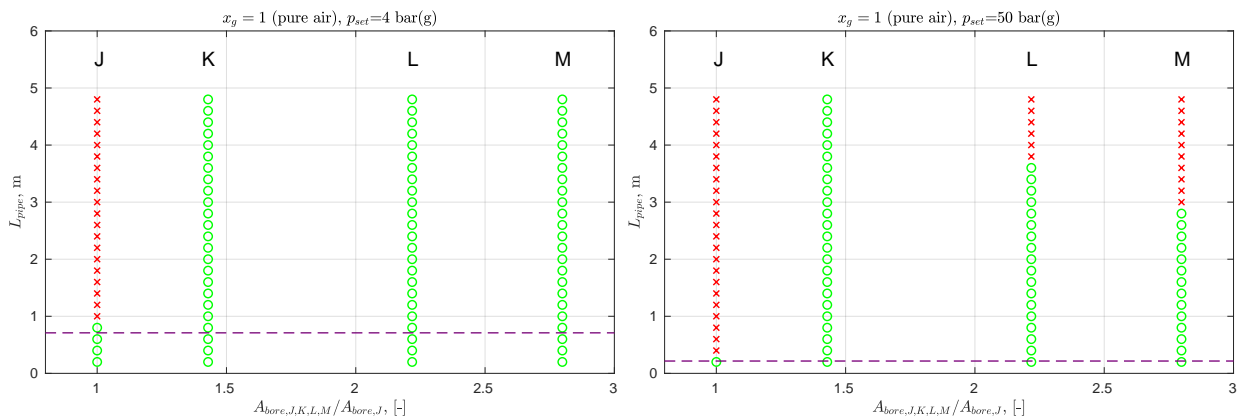


Fig. 7: Stability map of valve with orifices J, K, L and M at $p_{set} = 4$ and 50 bar, in air service.

We start by analysing the valve behaviour at air service. Fig. 7 depicts the stability properties at 4 barg and 50 barg (the 10 barg case was qualitatively the same as the 4 bar case). The horizontal axis depicts the orifice area ratios while the vertical axis is the pipe length. The horizontal dashed line show the analytical estimate Eq. (21) for the J orifice. Note that

for the rest of the orifices, one needs to recompute it; however, we depict the same value for all orifices to highlight the improvement. All valves vented the capacity of the J orifice at the prescribed pressure (e.g. approx. 1 kg/s at $p_{set} = 4$ barg), the required restriction was set as reported in Tab. 2. It is striking how the stability improves once restriction is applied, far beyond the critical pipe length (e.g. the J orifice goes unstable beyond approx. 0.8m, yet the K orifice – while venting the same mass flow rate – is stable up to pipe lengths of 5m). We stress that pipe friction was switched off in these simulations to keep different physical effects separated, as well as the influence of the effective area and lift-dependent discharge coefficient.

Similar improvement was experienced in the case of higher set pressure, see the right-hand-side panel of Fig. 7. Higher set pressures result in systems more prone to instability (the critical pipe length is shorter, see the horizontal dashed line); indeed, in this case, orifices L and M exhibit instabilities for longer pipes.

Fig. 8 depicts the same results for orifices in water service. It is interesting to observe that the stability boundary is higher than predicted by the analytical expression. This is due to the fact that Eq. (17) was developed for mid-lift cases (by perturbation around an equilibrium position), while in this case – as at the capacity flow rate the valves reach the upper stopper – no equilibrium exists in the dynamic theory sense (for further reading on this topic, we refer to Di Bernardo et al. (2008)). As in the water case, we see an improvement in the stability in the case of low set pressure (4 barg, left panel). However, in the case of high set pressure (50 barg, right panel) no improvement was found, rendering the restricted valves just as inadequate as the unrestricted, original J orifice.

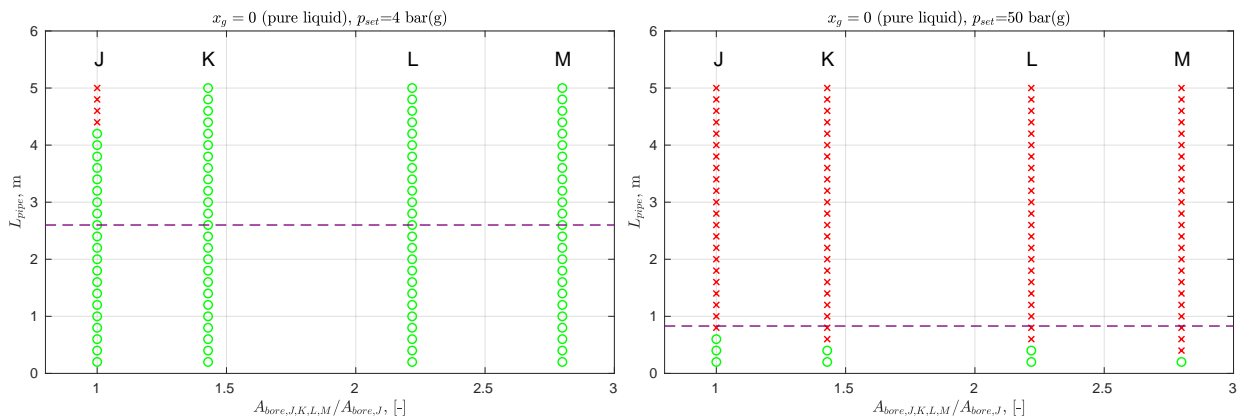


Fig. 8: Stability map of valve with orifices J, K, L and M at $p_{set} = 4$ and 50 bar, in water service.

To sum up, applying larger orifice with restriction seems to improve significantly the chatter situation in the case of gas service, which is probably due to the additional restoring force F_r . In the liquid case, the situation is more subtle; even though we experienced some improvement in the case of low set pressure, the restriction did not help if the set pressure was high. We speculate that this might be due to the hysteresis of valve chatter in the liquid case, that is, once the oscillation (chatter) is born, it immediately exhibits a large-amplitude oscillation that cannot be suppressed by re-setting the critical parameter value (in this case, pipe length), see H6s et al. (2016) for details. In mathematical terms, the Hopf bifurcation giving rise to the valve chatter is subcritical in the liquid case and supercritical in the gas case, see Kuznetsov (1998) for more details.

7 Conclusion

We have explored the effect of frozen mixture flow and restriction on valve chatter via numerical simulation and shown the importance of sonic velocity on valve stability and opening time. The following points can be concluded.

- Lower sonic velocities will result in slow valve motions and highly unstable valve operation.
- Mixtures of intermediate-mass fractions, i.e. extremely low sonic velocity, give rise to heavy valve chattering, even with short inlet piping.
- Both analytical formulae of opening time in Eq. (16) and critical pipe length in Eq. (17) provide simple means for an order-of-magnitude estimation even in the case of mixture flow, where the mixture sonic velocity is appropriately adjusted.
- The restoring force that emerges at the upper stopper of restricted valves assists in stabilizing the valves against chattering, notably in gas service (see Fig. 7), whereas it shows little (if any) improvement in terms of chattering in liquid service (see Fig. 8).

This study was the precursor of further investigation towards exploring the possibility of predicting valve dynamics and stability in the case of non-ideal and/or flashing fluids.

Acknowledgment and Funding Information

The research reported in this paper is part of project no. BME-NVA-02, implemented with the support provided by the Ministry of Innovation and Technology of Hungary from the National Re-search, Development and Innovation Fund, financed under the TKP2021 funding scheme.

References

- C. Alimonti, G. Falcone, and O. Bello. Two-phase flow characteristics in multiple orifice valves. *Experimental thermal and fluid science*, 34(8):1324–1333, 2010.
- J. D. Anderson. *Computational Fluid Dynamics*. Computational Fluid Dynamics: The Basics with Applications. McGraw-Hill Education, 1995. ISBN 9780070016859. URL <https://books.google.hu/books?id=dJceAQAIAAJ>.
- API. API 520, Sizing, Selection, and Installation of Pressure-Relieving Devices in Refineries Part II — Installation. *API*, 2015.
- C. Bazsó and C. J. Hős. An experimental study on the stability of a direct spring loaded poppet relief valve. *Journal of Fluids and Structures*, 42:456–465, 2013. ISSN 08899746. doi: [10.1016/j.jfluidstructs.2013.08.008](https://doi.org/10.1016/j.jfluidstructs.2013.08.008).
- G. Boccardi, R. Bubbico, G. P. Celata, and B. Mazzarotta. Two-phase flow through pressure safety valves. experimental investigation and model prediction. *Chemical Engineering Science*, 60(19):5284–5293, 2005.
- G. Boccardi, R. Bubbico, G. P. Celata, F. Di Tosto, and R. Trinchieri. Comparison among three prediction methods for safety valves design in two-phase flow in the case of a small valve. *Chemical Engineering Transactions*, 19:175–181, 2010.
- G. Burhani and C. Hős. Estimating the opening time of a direct spring operated pressure relief valve in the case of multiphase flow of fixed mass fraction in the absence of piping. *Journal of Loss Prevention in the Process Industries*, 66:104169, 2020.
- G. Burhani and C. Hős. An experimental study on the force coefficient and the discharge coefficient of a safety valve in air-water mixture flow. *Periodica Polytechnica Mechanical Engineering*, 65(4):326–336, 2021.
- C. Van Lookeren Campagne, R. Nicodemus, G. J. de Bruin, and D. Lohse. A Method for Pressure Calculation in Ball Valves Containing Bubbles. *Journal of Fluids Engineering*, 124(3):765–771, 08 2002. ISSN 0098-2202. doi: [10.1115/1.1486220](https://doi.org/10.1115/1.1486220).
- R. Darby. Size safety-relief valves for any conditions. *Chemical Engineering*, 112(9):42–50, SEP 2005. ISSN 0009-2460.
- R. Darby. The dynamic response of pressure relief valves in vapour or gas service. part 1: mathematical model, 2012. Proprietary report for PERF 99-05.
- W. Dempster and M. Alshaikh. An investigation of the two phase flow and force characteristics of a safety valve. *Procedia Engineering*, 130:77 – 86, 2015. ISSN 1877-7058.
- W. Dempster and M. Alshaikh. An Investigation of the Two Phase Flow and Force Characteristics of a Safety Valve. In Tu, ST and Chen, X, editor, *Pressure Vessel Technology: Preparing For the Future*, volume 130 of *Procedia Engineering*, pages 77–86, 2015. doi: [10.1016/j.proeng.2015.12.177](https://doi.org/10.1016/j.proeng.2015.12.177).
- M. Di Bernardo, C. Budd, A. Champneys, and P. Kowalczyk. Piecewise-smooth dynamical systems. theory and applications. 01 2008.
- M. Epstein, R. E. Henry, W. Midwidy, and R. Pauls. One-dimensional modeling of two-phase jet expansion and impingement. In *Proc. of the 2nd Int. Topical Meet. Nuclear Reactor Thermal-Hydraulics*, January 1983.
- I. Erdódi and C. Hős. Prediction of quarter-wave instability in direct spring operated pressure relief valves with upstream piping by means of cfd and reduced order modelling. *Journal of Fluids and Structures*, 73:37–52, 2017.
- M. Hellemans. *The safety relief valve handbook: Design and use of process safety valves to ASME and International Codes and Standards*. Elsevier, 2009.
- C. J. Hős, A. R. Champneys, K. Paul, and M. McNeely. Dynamic behaviour of direct spring loaded pressure relief valves connected to inlet piping: IV review and recommendations. *Journal of Loss Prevention in the Process Industries*, 48:270–288, JUL 2017. ISSN 0950-4230. doi: [10.1016/j.jlp.2017.04.005](https://doi.org/10.1016/j.jlp.2017.04.005).
- C. J. Hős, A. R. Champneys, K. Paul, and M. McNeely. Dynamic behavior of direct spring loaded pressure relief valves in gas service: Model development, measurements and instability mechanisms. *Journal of Loss Prevention in the Process Industries*, 31:70–81, 2014.
- CJ Hős, AR Champneys, K Paul, and M McNeely. Dynamic behaviour of direct spring loaded pressure relief valves: III valves in liquid service. 2016.
- B. Hughes. Consolidated 1900 series API 526 pressure relief valve, 2017. URL <http://www.bakerhughes.com>.
- H. Izuchi. Stability analysis of safety valve, 2010. American Institute of Chemical Engineers, *10th Topical Conference on Natural Gas Utilization ISBN: 9781617384417*.
- K. Kasai. On the Stability of a Poppet Valve with an Elastic Support. *Bulletin of JSME*, 11(48), 1968.
- D. K. Kim, H. E. Min, I. M. Kong, M. K. Lee, C. H. Lee, M. S. Kim, and H. H. Song. Parametric study on interaction of blower and back pressure control valve for a 80-kw class pem fuel cell vehicle. *International Journal of Hydrogen Energy*, 41(39): 17595 – 17615, 2016. ISSN 0360-3199.
- V. Kourakos, P. Rambaud, J. M. Buchlin, and S. Chabane. Flowforce in a safety relief valve under incompressible, compressible, and two-phase flow conditions (PVP-2011-57896). *Journal of Pressure Vessel Technology, Transactions of the ASME*, 2013. ISSN 00949930. doi: [10.1115/1.4006904](https://doi.org/10.1115/1.4006904).
- Y. A. Kuznetsov. *Elements of applied bifurcation theory*. Number 112 in Applied Mathematical Sciences. Springer, Berlin, 2 edition, 1998. ISBN 978-0387983820.
- F. Lees. *Lees' Loss prevention in the process industries: Hazard identification, assessment and control*. Butterworth-Heinemann, 2012.

- T. Lenzing, L. Friedel, J. Cremers, and M. Alhusein. Prediction of the maximum full lift safety valve two-phase flow capacity. *Journal of Loss Prevention in the Process Industries*, 11(5):307–321, 1998.
- J. C. Leung. A generalized correlation for one-component homogeneous equilibrium flashing choked flow. *AIChE Journal*, 32(10): 1743–1746, 1986.
- J. C. Leung. Similarity between flashing and nonflashing two-phase flows. *AI Ch. E. Journal (American Institute of Chemical Engineers);(USA)*, 36(5), 1990.
- J. C. Leung. The omega method for discharge rate evaluation. In *International symposium, Runaway reactions and pressure relief design*, pages 367–393, The address of the publisher, 1995. DIERS, AICHE. ISBN: 0816906769.
- J. C. Leung. A theory on the discharge coefficient for safety relief valve. *Journal of Loss Prevention in the Process Industries*, 17(4):301–313, 2004.
- J. C. Leung and M. A. Grolmes. A generalized correlation for flashing choked flow of initially subcooled liquid. *AIChE Journal*, 34(4):688–691, 1988. doi: [10.1002/aic.690340421](https://doi.org/10.1002/aic.690340421).
- J. C. Leung and F. N. Nazario. Two-phase flashing flow methods and comparisons. *Journal of Loss Prevention in the Process Industries*, 3(2):253–260, 1990.
- G. M. Makaryants. Fatigue failure mechanisms of a pressure relief valve. *Journal of Loss Prevention in the Process Industries*, 48: 1–13, 2017.
- P. Meena, S. Rittidech, and N. Poomsa-ad. Application of closed-loop oscillating heat-pipe with check valves (clohp/cv) air-preheater for reduced relative-humidity in drying systems. *Applied Energy*, 84(5):553 – 564, 2007. ISSN 0306-2619.
- G. A. Melham. Analysis of PRV stability in relief systems, part I. Detailed dynamics, 2014. An ioMosaic Corporation White Paper.
- P. Moussou, R. J. Gibert, G. Brasseur, Ch. Teygeman, J. Ferrari, and J. F. Rit. Instability of Pressure Relief Valves in Water Pipes. *Journal of Pressure Vessel Technology*, 132(4):041308, 2010. ISSN 00949930. doi: [10.1115/1.4002164](https://doi.org/10.1115/1.4002164).
- T. Narabayashi, H. Nagasaka, M. Niwano, and Y. Ohtsuki. Safety relief valve performance for two-phase flow. *Journal of Nuclear Science and Technology*, 1986. ISSN 00223131. doi: [10.1080/18811248.1986.9734973](https://doi.org/10.1080/18811248.1986.9734973).
- K. Ng and C. Yap. An investigation of pressure transients in pipelines with two-phase bubbly flow. *International journal for numerical methods in fluids*, 9(10):1207–1219, 1989.
- D. L. Nguyen, E. R. F. Winter, and M. Greiner. Sonic velocity in two-phase systems. *International Journal of Multiphase Flow*, 7(3):311–320, 1981. ISSN 0301-9322. doi: [https://doi.org/10.1016/0301-9322\(81\)90024-0](https://doi.org/10.1016/0301-9322(81)90024-0). URL <https://www.sciencedirect.com/science/article/pii/0301932281900240>.
- A. Singh. An analytical study of the dynamics and stability of a spring loaded safety valve. *Nuclear Engineering and Design*, 72(2):197–204, 1982.
- A. Singh. On the stability of a coupled safety valve-piping system. *Thermal-hydraulics of nuclear reactors, paper presented at the second int. topical meeting on nuclear reactor thermal-hydraulics*, 1983.
- F. Zheng, C. Zong, C. Zhang, X. Song, F. Qu, and W. Dempster. Dynamic instability analysis of a spring-loaded pressure safety valve connected to a pipe by using computational fluid dynamics methods. *Journal of Pressure Vessel Technology*, 143(4), 2021.